Hindawi
Advances in Civil Engineering
Volume 2019, Article ID 1829124, 15 pages
https://doi.org/10.1155/2019/1829124

Research Article

Experimental Investigation on the Influence of Regional Concrete Spalling on Shield Tunnel Segments

Shimin Wang, Chuankun Liu, Gaoyu Ma, Songyu Cao, Junbo Zhang, Daiyue Lu, and Chuan He

Key Laboratory of Transportation Tunnel Engineering Ministry of Education, Southwest Jiaotong University, Chengdu 610031, China

Correspondence should be addressed to Songyu Cao; caosongyu@my.swjtu.edu.cn

Received 1 April 2019; Revised 22 May 2019; Accepted 27 May 2019; Published 27 June 2019

Academic Editor: Amir Si Larbi

Based on the field investigation and analysis, the mechanical characteristics of segment structure in shield tunnels are compared and analyzed under the circumstances of different concrete spalling region by the method of similarity model experiment. Through data analysis of acoustic emission, the results for displacement and internal force of shield tunnel segments are clarified on the segment lining, the influential rule of load bearing capacity is also determined, and the deformation and stress for the different concrete spalling region are described as well. The corresponding research results indicate that range for elastic bearing stage is enlarged while it is narrowed for plastic bearing stage, the convergence and deformation and the accumulated event numbers for acoustic emission on critical instability point are obviously increasing, and the process of damage and failure tends to be sudden for segment lining structure. The ultimate bearing capacity of the damaged segment lining obviously decreases due to regional concrete spalling; to be more specific, the reduction rate for ultimate bearing capacity becomes 6%, 6%, and 13%, respectively, when the range of concrete spalling reaches 45°, 60°, and 75°.

1. Introduction

In the process of shield tunnel construction, because of the influential factors such as the geological condition, the construction design, and the bias load, it is unavoidable during tunnel construction for the occurrence of segment cracking, damage, and regional concrete spalling [1, 2], of which regional spalling for concrete segment is the most prominent disease against structure performance and safety in shield tunnel. Furthermore, regional spalling is primarily distributed in the area adjacent to the joints between segment rings, and the disease is commonly manifested as strip shape along the circumferential joints of segments, even resulting in the exposure of steel bar in a more severe condition. As a matter of fact, the water-proof property, the load bearing capacity, and the long-term durability of segment lining structure will be dramatically affected [3].

At present, various degrees of damage problems have been observed during construction and service period for a large number of shield tunnels. Combined with the specific projects, scholars have conducted a large amount of researches on the influential factors of structural damage for segment lining and the corresponding controlling measures are proposed in the perspective of stratum condition, stratum defects, and unfavorable load condition during construction. Li et al. have collected a mass of disease specimens for shield tunnels and have established TSI comprehensive tunnel service index for the evaluation of disease condition in shield tunnel by the regression formula of least square method [4]. Leung and Meguid have analyzed the variation of the earth pressure distribution after the occurrence of cavity for different locations around existing tunnels [5]. Lei has analyzed the stress distribution, the changing rule, and the lining failure process in tunnel structure and surrounding rocks for shallow-buried tunnels under the action of unsymmetrical load with different bias angle through model test [6]. Amedeo Manuello has carried out real-time research on the damage evolution of two arch units for precast concrete on certain highway tunnel and has analyzed the cracking and damage mode using multichannel

acoustic emission acquisition system which is able to wirelessly transmit and process data on the spot [7]. Xin et al. have investigated the tension and compression stress and the damage mode for the proportional tunnel model, respectively, with and without lining headspace by conducting research on the dynamic behavior of tunnel structure based on shaking table [8]. Mo and Chen have conducted numerical simulations for segment cracks during construction and service stage by software ADINA and ANSYS, respectively, and have analyzed the expansion law of the cracks in the vicinity of bolt hole; then, the corresponding method has been put forward on the promotion of crack resistance property for concrete [9, 10]. He and Liu have illuminated the effect of different crack numbers, length, and position on the structural mechanical property of segment in shield tunnel [11, 12]. Feng et al. studied the mechanical properties of the single-layer and double-layer lining structures under hydrostatic water pressure and the interaction between the lining and the stratum through model tests and field tests [13]. Fang et al. have analyzed the mechanical property of segment lining for the shield tunnel segment of Lanzhou metro across Yellow River by the method combined with model test and numerical simulation [14]. Liu et al. have conducted full-scale experiment focusing on the segment in quasirectangular shield tunnel and analyzed the effects of reinforcement of "T"-shaped section, the position of longitudinal joints, and the shear capacity on the structural mechanical property [15, 16]. Zhou et al. have completed laboratory impact test by the equipment application for drop hammer test of synchronous measuring system and have analyzed the effect of loading direction on the failure mode of cracked tunnel [17]. Wang et al. have analyzed the effect of stratum cavity and different water pressure on the failure mode and the bearing capacity of shield tunnel structure [18, 19]. Kohno et al. introduced a two-state availability model to discuss the overall safety of a tunnel project [20]. Zhang et al. employed an axisymmetric model representing plate-like concrete such as slabs, walls, and tunnel linings. The effect of material properties (intrinsic permeability and porosity) and environmental condition (saturation degree) on spalling was investigated [21]. Luo et al. developed a series of true-triaxial tests on cube specimens with a D-shaped hole and summarized the process and failure characteristics of sidewall spalling and discussed the influence of cross-sectional shape on tunnel failure characteristics and tunnel stability [22]. Gong et al. reproduced the process of rockburst induced by spalling damage in deep hard-rock tunnels and revealed the mechanism by which spalling damage induces rockburst through a true-triaxial test system [23].

Most of the existing research achievements are focusing on the crack generation and expansion in the process of segment failure; so far, relevant reports are not displayed aiming at the effect of regional concrete spalling in the aspect of structural bearing capacity and mechanical behavior. In this paper, a subway project is taken as the background, based on the field investigation and analysis for the situation of regional concrete spalling and the mechanical characteristics of segment lining structure under the circumstances with different concrete spalling region by similarity test, and the conclusion can be provided as the theoretical proof for the design optimization, disease analysis, and shield tunnel evaluation.

2. Background Analysis

2.1. General Situation of the Project. The stratum is complicated and flexible in the crossing range of the metro tunnel, and the soil property is cross distributed from north to south, which is specifically presented in sequence as hard-soft-hard-soft-hard-soft-hard-soft-hard, and the proportion of crossed soft soil for the whole section accounts for 56.4%. The soil layer property is defined as compound stratum with a relatively large proportion of soft soil, and the tunnel construction underneath passes across multiple surface water. The section profile of the damaged segment lining is shown in Figure 1, and the stratum component is indicated consecutively from top to bottom as miscellaneous fill, silt, clay, silt, silty clay, residual silty clay, and residual gravel clay. The left side of the interface between soft rock and hard rock is consisted of completely weathered granite, while the right side is composed of residual gravel clay. When crossing the upper-soft lower-hard stratum during tunnel construction, tunneling posture will be affected, consequently resulting in poor boring attitude which could more likely cause uneven Jack thrust and bias load on segments, and boring attitude problem is also one of the most prominent factors for segment damage during construction.

2.2. Structural Form. The outer and inner diameters of the cross-river tunnel for the metro project are 6.2 m and 5.5 m, respectively. The segment thickness is 0.35 m, and the width is 1.2 m. "3 + 2 + 1" blocked mode is adopted for the segment lining, of which standard block accounts for 67.5°, adjacent block accounts for 68.75°, and the key block accounts for 20°; staggered assembly is applied for the segment, and for each ring, 16 longitudinal bolts are distributed and arranged with equal angle. As presented in Figure 2, rebate is set up between segment rings, the width for the end region of tenon is 127 mm, and the width for the interior of groove is 135 mm; 8 mm free fitting allowance is designed for the connection of segment rings between tenon and mortise. The tongue-and-groove structure could partially increase the longitudinal stiffness of tunnel structure, which is commonly placed for the straight-jointed segment in uniform soft soil stratum. In consequence, higher requirement for assembly accuracy is needed; once assembly errors exceed the limit value, the degree of stress concentration will be dramatically increased for the rebate area of segment, resulting in cracks, even extensive concrete spalling. In this project, staggered-jointed assembly is applied, and the requirement for assembly accuracy of stagger-jointed assembly will be even higher compared with straight-jointed assembly, and consequently, the probability for segment damage is increased due to unfavorable construction load when crossing upper-soft lower-hard stratum. Therefore, in upper-soft lower-hard stratum, the arrangement of rebate and the application of

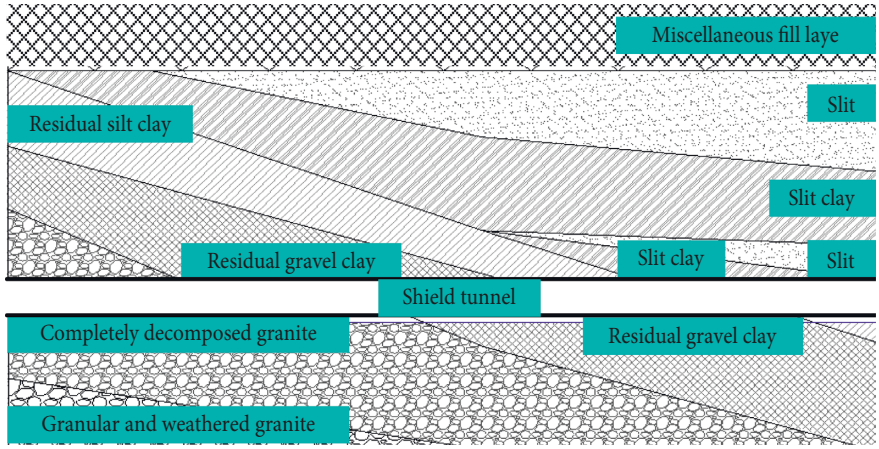

Figure 1: Cross section formation condition.

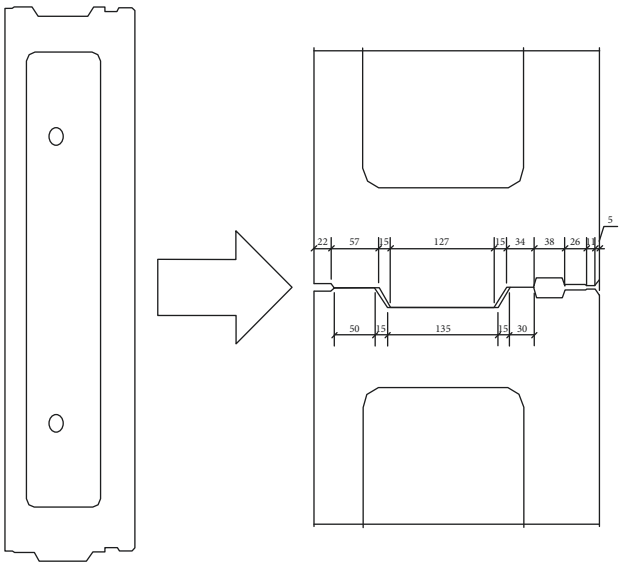

Figure 2: Sketch of tenon between segment rings (unit: mm).

stagger-jointed assembly will be the vital factors for segment damage during construction.

2.3. The Investigation and Analysis for the Disease of Concrete Spalling for Partial Segment. The overall length of this investigated tunnel section is 3.61 km, totally 3008 rings are observed in the investigated area, and up to 443 damaged places are recorded. According to the characteristics of geometrical form, the damage form for the disease of shield tunnel segment can be divided into 3 categories which are, respectively, corner damage, longitudinal cracks, and regional concrete spalling, and the greatest value for the numbers of each individual disease among them is summarized for regional concrete spalling which amounts to 203 and accounts for 45.8% of all the diseases observed in tunnel; undoubtfully, the severity for concrete spalling is the most.

In this metro project, all of the regional concrete spalling takes place around the circumferential joints between segment rings, mostly occurred in the posterior part of segments along excavation direction, and distributed symmetrically on the vault along circumferential direction. Besides, as presented in Figure 3, the disease generally occurs accompanied with circumferential dislocation between segment rings. And the regional concrete spalling along segment rings is shown in Figure 4. The concrete spalling is concentrated in the range of 45° from the left and right side of the vault, while the distribution is relatively lesser on the bottom of the arch and tends to be identical between the left and right haunch.

The statistical result is presented in Table 1 for the length, width, and depth of regional concrete spalling, the corresponding average arc length comes to 1443 mm along the circumferential direction, which accounts for half length of the inner arc of the segment, and the maximum value reaches 3190 mm. Obviously, the disease has already spread over the posterior part of the segment along segment ring and even extended to the adjacent segments. The average width is 183 mm for regional concrete spalling, and the width between the margin of the segment and the hand hole is 196 mm, indicating that the region of concrete spalling almost approaches to the periphery of the hand hole. The corresponding maximum value for the width reaches to 230 mm, which means the inner edge of hand hole has already been extended to, and as a matter of fact, the mechanical behavior for the hand hole of the segment is affected, and more severely, structural failure for the segment may be caused. The average depth is 94 mm for regional concrete spalling and has exceeded 1/4 of the segment thickness. The distributions for length, width, and depth of the regional concrete spalling for segments are presented in Figure 5; the length of regional concrete spalling is mostly observed from 70 mm to 1000 mm, while the width is concentrated from 100 mm to 230 mm.

3. Similarity Model Test

3.1. Determination of Similarity Basis. 11/12 geometrical similarity ratio and 1/1 unit weight similarity ratio are taken as the basic similarity ratios, $C_u = C_g = C_\varphi = 1$ is used for

(a) (b)

Figure 3: The investigated picture for the disease of concrete spalling on the scene. (a) Multiple successive ring spalling on the vault. (b) Regional concrete spalling.

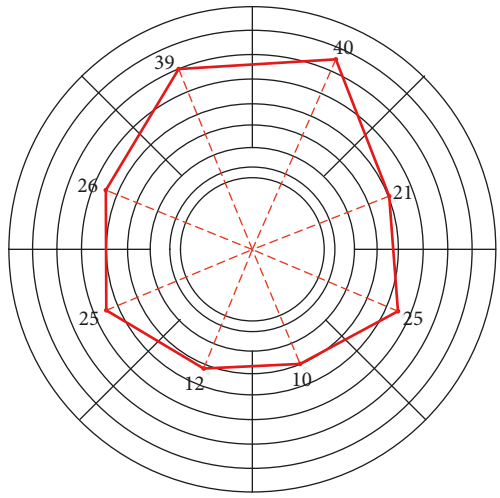

Figure 4: Distribution of spallings in the circumferential region along segment ring.

Table 1: Statistical results of the length, width, and depth of spallings.

Characteristic value	Length (mm)	Spalling angle (°)	Width (mm)	Depth (mm)
Maximum value	3190	66.46	230	118
Minimum value	60	1.25	50	12
Average value	1443	30.06	183	94

Poisson's ratio, stress and frictional angle are deduced according to similarity theory, and $C_R = C_\sigma = C_c = C_E = 12$ is applied for similarity ratio of strength, stress, cohesive force, and elasticity modulus.

3.2. Design for Similarity Model. The cross-river shield tunnel excavation has encountered various stratums with different buried depth, water pressure, and the degree of softness and hardness. The effect due to construction is not taken into consideration for the test while the test is mainly focusing on the mechanical characteristics after the damage of the segments; therefore, the most undesirable soil body towards the stability of the structure is selected as the prototype soil which is specified as silty clay, eluvial silty clay, eluvial sandy clay, and the primary controlling parameters such as unit weight, elasticity modulus, and cohesive force are confirmed. Mainly, fly ash and river sand are taken as the similarity materials, and certain proportional hot-melt mixture is used, which is consisted of crystal powder, coarse quartz sand, fine quartz sand, petroleum jelly, rosin, and engine oil. The mix proportion is maintained being adjusted until the parameters of physical mechanics reach the expectation value for the material of soil model. The mix proportion and the parameters of physical mechanics for the material of soil model are indicated in Tables 2 and 3.

The strength grade for the segmental concrete is C50. In the model test, plaster is chosen as the basic material for the segment model, and certain proportional diatomite is mixed. The proportion of the materials is trial-produced by the adjustment of ratio between water and plaster, and the proportion is evaluated by the data of uniaxial compressive strength test. Finally, the ratio between water, plaster, and diatomite will be determined as 1 : 1.38 : 0.1, and these materials will be applied for the segment lining structure. The parameters of physical mechanics for segment concrete are shown in Table 4.

The diameter of the mesh reinforcement is chosen as 1.3 mm for the circumferential main reinforcement, and the simulation is conducted according to the principle of equivalent bending stiffness. For the intermediate ring of the model, respectively, 4 iron wires are applied for the main reinforcement simulation on both inner side and outer side of the segment. The main reinforcement for the circumferential segment is shown in Table 4. After the process of prefabrication and demoulding, the segment lining is maintained under the condition of certain temperature and humidity.

The simulation of segmental joint can be divided into circumferential joint simulation and longitudinal joint simulation, of which the weakening effect of bending stiffness for the joint is simulated by the incision on the place of circumferential joint along depth direction. The groove depth of incision is determined by the principle of equivalent bending resistance of prototype joint [24]. The matching

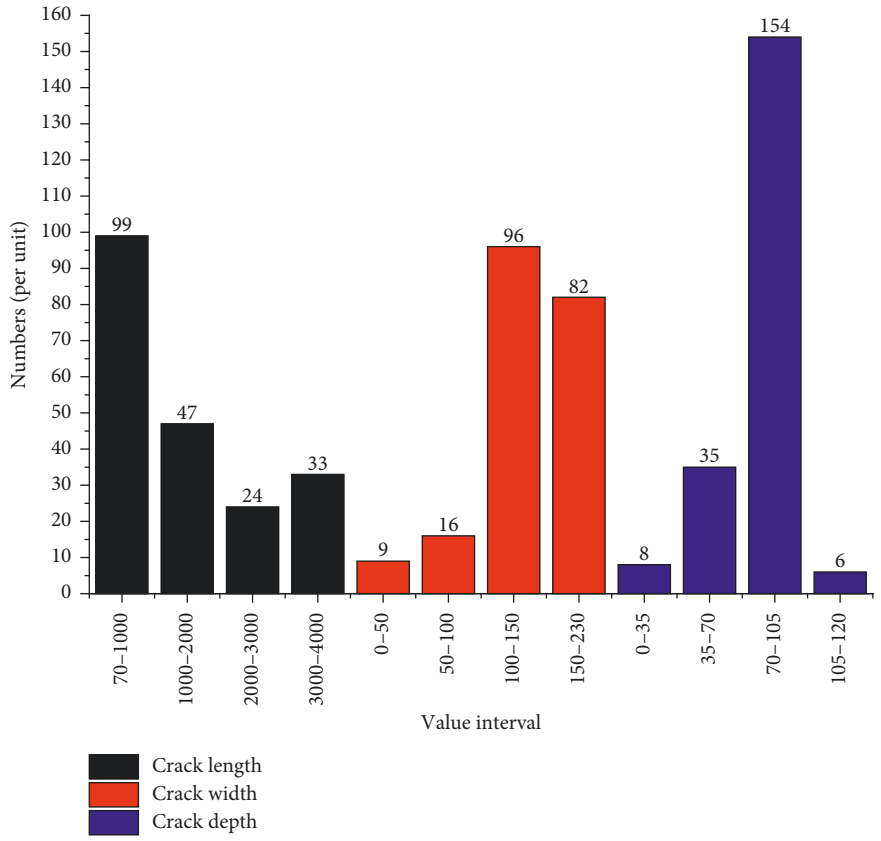

Figure 5: Length, width, and depth for the regional concrete spalling of segments.

Table 2: Mix proportion of model soil.

Crystal powder	Fine quartz sand	Coarse quartz sand	Engine oil	Fly ash	River sand	Petroleum jelly	Rosin
1	0.35	0.35	0.15	0.35	0.65	0	0.06

Table 3: Physical and mechanical parameters of soil.

Parameter	c (MPa)	Φ (°)	E (MPa)	γ (kN·m^{-3})
Prototype material	18.1~21.9	7.9~11.3	4.6~6.1	17.2~19.0
Model material	1.67	9	0.42	18
Corresponding prototype value	20	9	5	18

Table 4: Physical and mechanical parameters of segment concrete.

Parameters of physical mechanics	Prototype value	Model value	Corresponding prototype value
Elasticity modulus (GPa)	34.5	2.875	34.4
Standard value for uniaxial compressive strength (MPa)	32.4	2.7	32.0
Equivalent compressional stiffness for the circumferential main reinforcement (N)	2.434e9	1.803e5	2.817e9

situation is shown in Table 5 between the groove depth for the joint of the segment model and the bending stiffness of prototype joint. The placement for groove of segment joint is presented in Figure 6.

Considering the longitudinal assembly effect, the model is assembled by 3 rings which are consisted of one integral segment ring and two half-width segment rings along longitudinal direction. As shown in Figure 7, the intermediate ring is chosen as the target ring for analysis. As for the longitudinal joint, it is assumed that no dislocation occurs. The simulation method is presented as follows: the longitudinal joint between the two segment rings is connected by a steel rod with a diameter of 4 mm and a length of 40 mm and bonded with epoxy resin.

Table 5: Gap depth of segment transverse joints.

Bending stiffness (N·m·rad^{-1})		Groove depth for entity (m)	Groove depth for model (m)
Positive bending	2.44×10^8	0.14	0.023
Negative bending	1.46×10^8	0.16	0.026

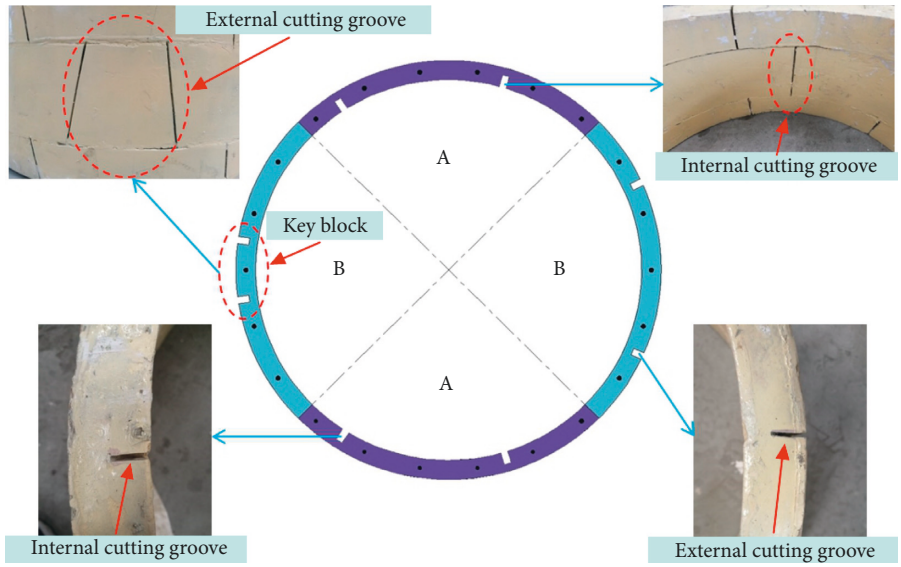

Figure 6: Groove of partition for segment joint.

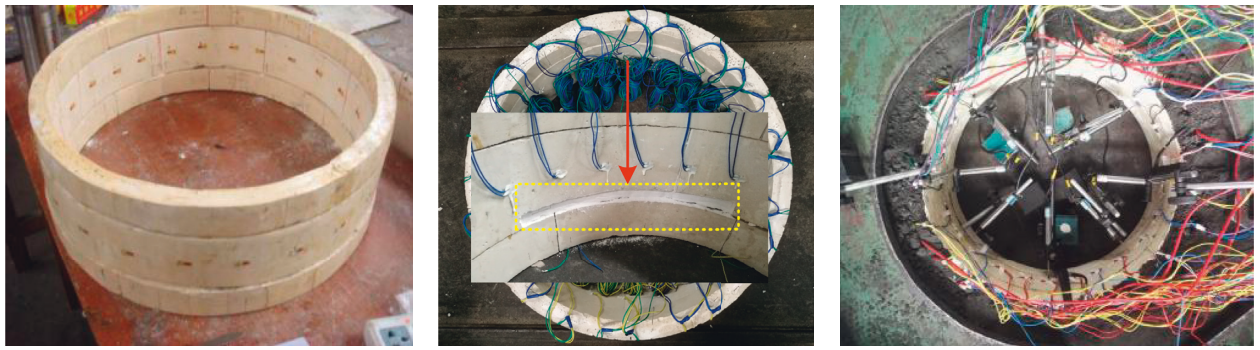

(a) (b) (c)

Figure 7: Fabrication and installment for the segment model of regional concrete spalling. (a) Model fabrication. (b) Arrangement for regional spalling. (c) Model installment.

3.3. Test Grouping. According to the distribution results of the spalling angle corresponding to spalling length in the process of field investigation, the location of regional concrete spalling is arranged at the vault position and symmetrically distributed along ring direction relative to the axis of vault in the experiment. Four cases with different spalling ranges are arranged, and the ranges are set to 0°, 45°, 60°, and 75°, respectively. The statistical average values are selected for the spalling width and depth, namely, 183 mm and 94 mm; the grouping situation of the test is shown in Figure 7. During the test process, regional concrete spalling is achieved by removing the corresponding part from the posterior border of the segment according to the spalling length, width, and depth in test scheme, and the grouping is shown in Table 6.

3.4. Test Equipment and Loading Mode. The model test is carried out by "Combined tunnel-stratum loading test system." As presented in Figure 8, the fabricated model is firstly placed on the center of baseplate in the process of the test, and the space between the model and the loading plate along horizontal direction will be filled with soil specimen, and then loading plate along direction III will be applied for covering the soil and ring model on the top. Operating hole will be reserved at the corresponding place of test model on loading plate along direction III for the convenience of operation, observation, and data recording in the test process. For the guarantee of plane strain stress, originally loading along direction III is applied; then the loading ratio along directions I and II will be confirmed according to the equation: $\lambda = 0.5$ where λ is the stratigraphic lateral pressure

Table 6: Groups of test schemes.

Grouping number	Assembly method	Center point for the target block "F"	Range of regional spalling	Spalling length (mm)	Spalling width (mm)	Spalling depth (mm)
1	Relatively rotate 180°between segment rings	45°left to the bottom of the arc	None	0	0	0
2			45° at vault	2159.8	15.5	8.0
3			60° at vault	2879.8	15.5	8.0
4			75° at vault	3599.7	15.5	8.0

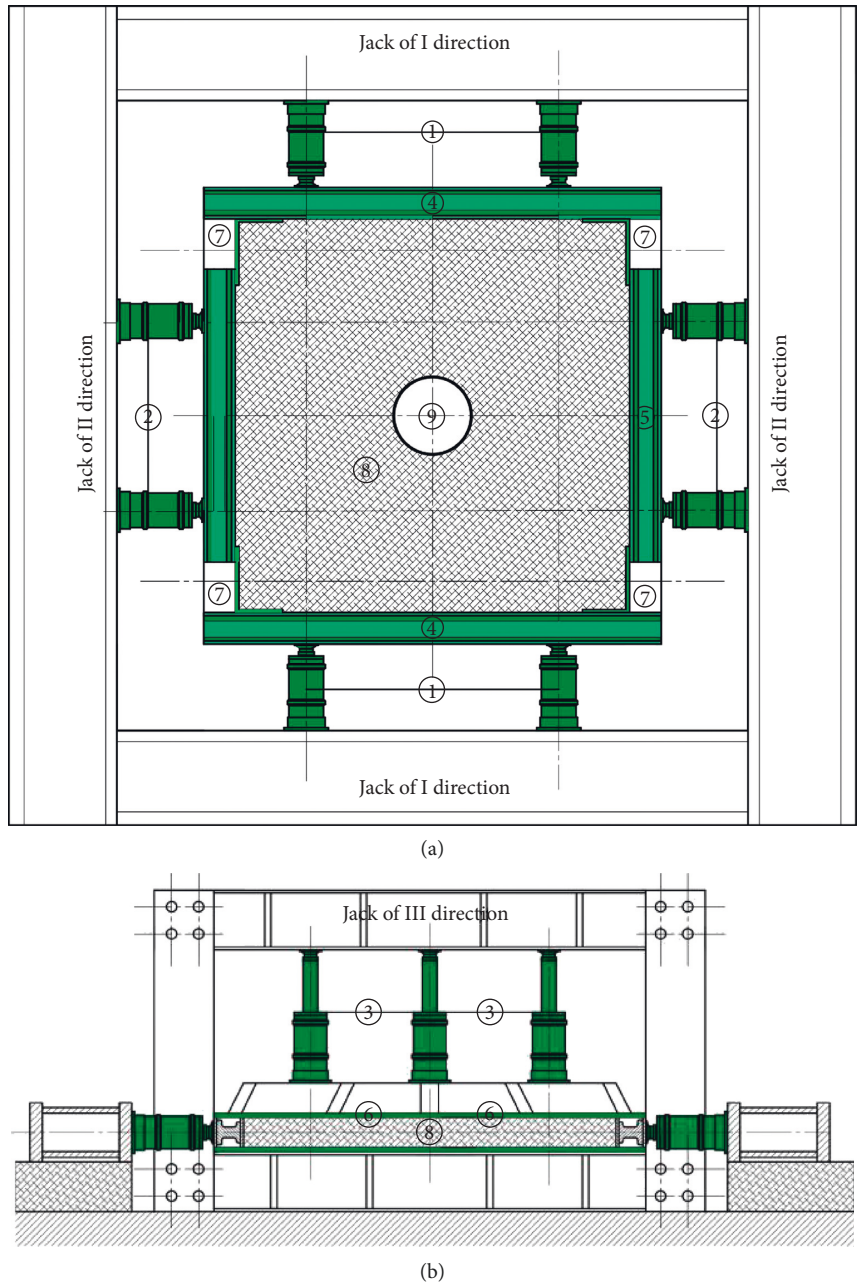

Figure 8: Loading device. (a) Vertical view of the loading device. (b) Lateral view of the loading device. ①Jack of direction I. ②Jack of direction II. ③Jack of direction III. ④Plate of direction I. ⑤Plate of direction II. ⑥Plate of direction III. ⑦Loading plate. ⑧Surrounding soil. ⑨Model segment.

coefficient. Both earth pressure along direction I and direction II will be applied to operating state by step loading mode; then factors such as structural degradation and overloading will be simulated by the continued step loading of earth pressure until the occurrence of unstable failure towards segment structure. The magnitude of the step

loading value is obtained by theory calculation, as briefly presented in Table 7. In the test, the intermediate ring model is considered as the measured object, 24 sets of resistance strain gauges are arranged, respectively, for the inner and outer side of the segment ring with equal angle, and 8 displacement gauges are arranged with identical interval along the inner side of the intermediate ring. Meanwhile, 1probe for acoustic emission is placed, respectively, on the vault, bottom of the arc, the left haunch, and the right haunch.

4. Analysis for Test Results

4.1. Message Analysis for Acoustic Emission. It is shown in Figure 9 for the variation of event numbers for acoustic emission with the change of load step in the process of loading for different groups of segment rings. The accumulated event numbers for acoustic emission are relatively minor from the beginning of loading to loading level 5, which indicates that this stage is considered as elastic stage for segment lining, and no obvious damage has not been observed yet; from loading level 5 to loading level 16, local failure and damage occur in the segment lining; besides, step-shaped increase is observed for the accumulated event numbers of acoustic emission in this stage, which presents that the existence of regional concrete spalling will intensify the damage and failure degree of the segments. When the range of concrete spalling reaches up to 75°, step-shaped increase will also tend to occur for the event number of accumulated acoustic emission from loading level 6 to loading level 15; however, the stage height is gradually increasing while the number of stages is obviously reduced, which shows that the expansion speed of the damage and failure for the segment lining in this stage is accelerated.

The integral stiffness of the structure is reduced due to the existence of regional concrete spalling compared with undamaged segment rings. According to the comparison analysis for the test segments with different range of concrete spalling from group 1 to group 4, while the flexibility of segment lining is increased, the corresponding range of elasticity capacity is augmented as well. The numbers for the gradually formed step shape are reduced for the accumulated event numbers of acoustic emission with the increase of load step and the stage height also gradually increases, indicating a sudden change for the process of damage and failure of segments.

4.2. Analysis for the Displacement of Segment Lining. According to the displacement value of the vault, bottom of the arch, and the left and right haunches for different groups of segment lining, the variation curve of lateral and vertical convergence value is obtained for different groups of segment lining by statistical method, which is shown in Figure 10. The shorten is considered as positive while the extension is deemed negative for the convergence value of segment lining structure. According to Figure 10, gradual increases for the groups of segment linings are observed with the increase of loading for the lateral and vertical convergence value. Compared with undamaged segment lining structure, the magnitude for deformation value is obviously increased under the action of identical loading due to the existence of regional concrete spalling, and the growing rate for the convergence value of segment lining is increasing with the expansion of regional concrete spalling. Moreover, the amplification for convergence value is significantly increased with the increases of loading level. Because the position of concrete spalling region is on the vault, the weakening of vertical stiffness for segment lining structure will be more prominent. Furthermore, the variation trend of vertical convergence value is more remarkable compared with that of lateral convergence value for segment lining structure.

As shown in Figure 11, for the variation situation of elliptical aspect ratio for the groups of test segments, the whole elliptical changing characteristics can be briefly described by the aspect ratio of ellipse for segment lining. Compared with undamaged lining structure, the aspect ratio of ellipse will be conspicuously increased before and after instability due to the existence of regional concrete spalling. From the beginning of initial loading to the stage in which the instability almost occurs, the growth rate of elliptical aspect ratio tends to be smooth for the undamaged segment rings, which indicates that the deformation of segment lining is relatively smaller compared with damaged ones, and the corresponding integral ability to resist deformation is relatively stronger, while the segment deformation is comparatively greater before and after instability for the segments under the effect of concrete spalling. Besides, the growing rate of elliptical aspect ratio for damaged segment is relatively more obvious.

To have a better description of the change law, for the different groups of segment rings, it is summarized in Table 8 for the demarcation point between elasticity and plasticity, for the critical point of instability, and for the results of elliptical aspect ratio. Compared with undamaged segment lining structure, effective cross-sectional area in spalling area is reduced by concrete spalling, and consequently, the integral bending stiffness will be decreased as well. As a matter of fact, the degree of stress concentration for the inner side of the structure will be relieved by the occurrence of greater displacement under the action of identical external load on segment lining. The range for the stage of elastic bearing capacity will be minorly increased with the range expansion due to segmental concrete spalling, while the range for plastic bearing stage is obviously reduced. The increments for the vertical convergence of the elastic-plastic demarcation point are recorded as 143.43%, 198.86%, and 208.57%, respectively, for the damaged segment under the effect of concrete spalling compared with undamaged segment rings by comparison and analysis of the different concrete spalling ranges for the vertical and lateral convergence value of segment lining, and the corresponding increments for lateral convergence are recorded as 3.92%, 7.04%, and 16.2%, the increments of elliptical aspect ratio are 47.78%, 66.67%, and 76.67%, respectively; the increments for the vertical convergence critical point of instability are 83.17%, 91.42%, and 95.30%, the corresponding increments

Table 7: Test load applying scheme.

Loading step	Jack pressure of direction III (MPa)	Load of direction I		
		Jack pressure (MPa)	Formation pressure of the model vault (kPa)	Formation pressure of the prototype vault (kPa)
0	0	0	0	0
1	4	2	2.7	32.4
2	6	4	6.5	78.0
3	8	6	10.4	124.8
4	10	8	13.9	166.8
5	12	10	17.3	207.6
6	14	12	20.9	250.8
7	16	14	24.2	290.4
8	17	16	28.3	339.6
9	18	18	31.6	379.2
10	18	19	35.3	423.6
11	18	20	38.7	464.4
12	18	21	42.2	506.4
13	18	22	45.8	549.6
14	18	23	49.6	595.2
15	18	24	53.5	642.0
16	18	25	56.9	682.8
17	18	26	60.6	727.2
18	18	27	64.8	777.6

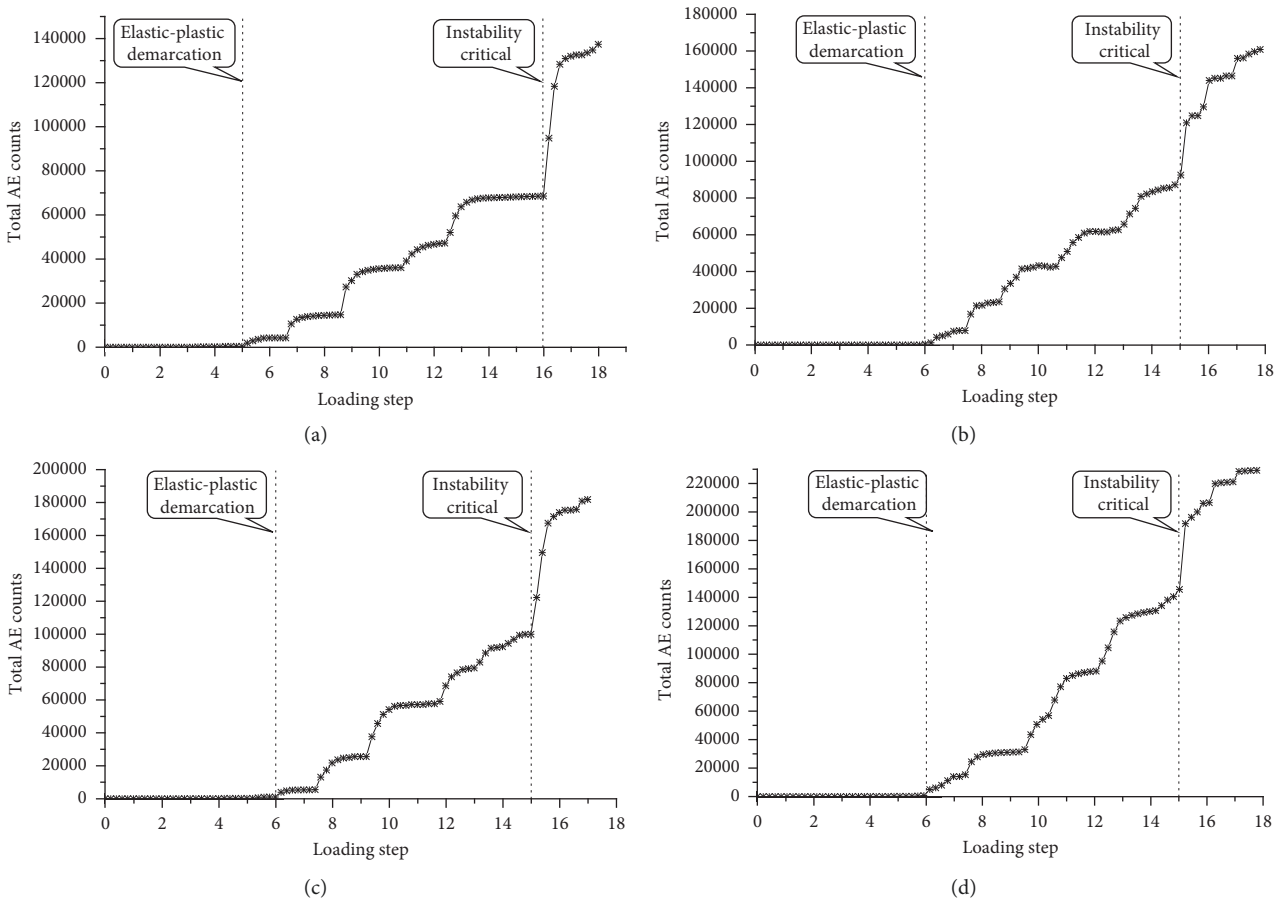

Figure 9: Segment AE test results. (a) Variation curve of acoustic emission for group 1. (b) Variation curve of acoustic emission for group 2. (c) Variation curve of acoustic emission for group 3. (d) Variation curve of acoustic emission for group 4.

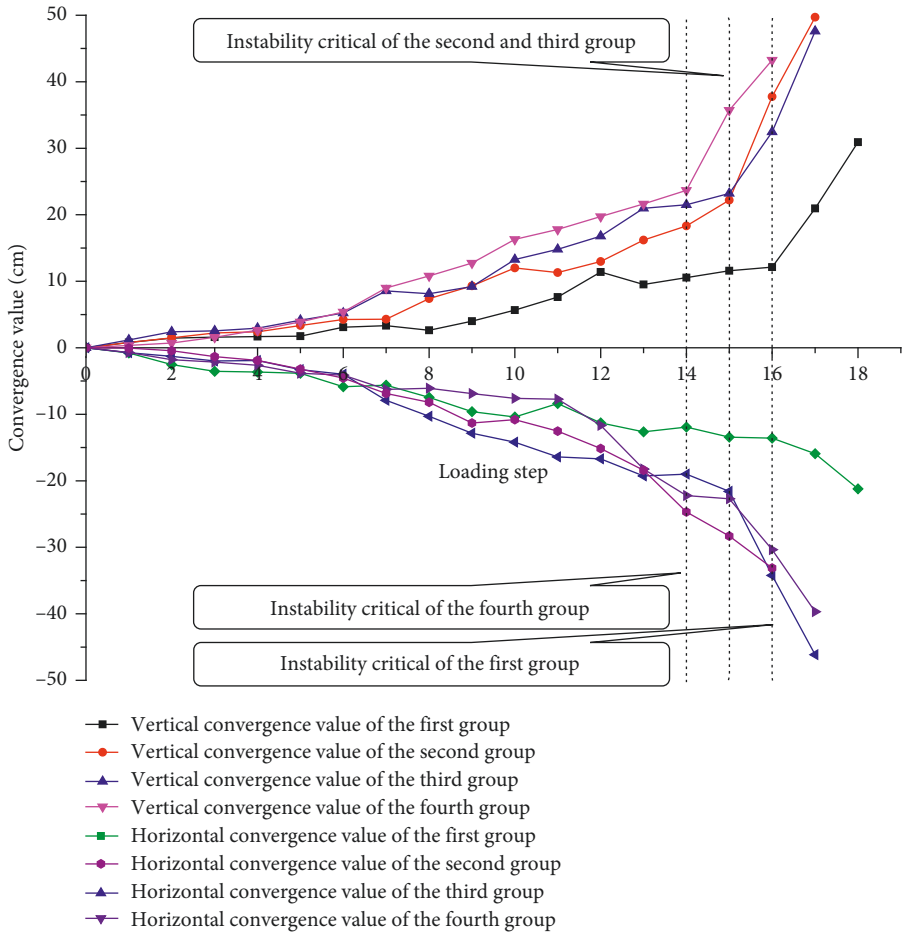

Figure 10: Convergence value of horizontal and vertical directions of segment lining.

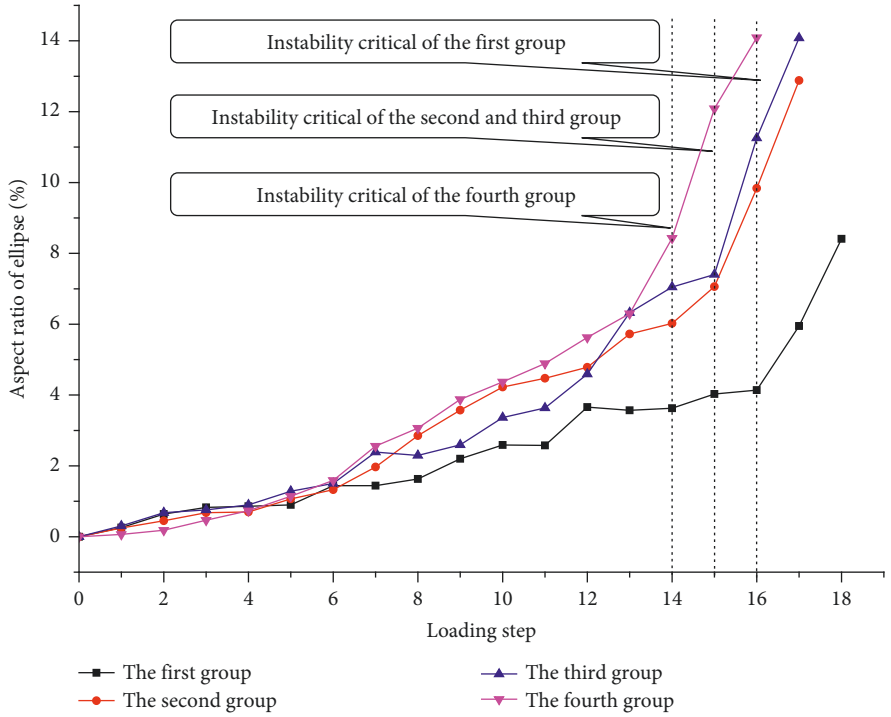

Figure 11: Elliptical aspect ratio for groups of test segment.

Table 8: Deformation of each group of segment.

Group number	Range of regional spalling	Elastic-plastic demarcation point				Critical point for loss of stability			
		Corresponding loading step	Vertical convergence (cm)	Lateral convergence (cm)	Elliptical aspect ratio (%)	Corresponding loading step	Vertical convergence (cm)	Lateral convergence (cm)	Elliptical aspect ratio (%)
1	无	5	1.75	3.83	0.90	16	12.12	13.58	4.15
2	45°	6	4.26	3.98	1.33	15	22.20	21.58	7.06
3	60°	6	5.23	4.10	1.50	15	23.20	22.70	7.40
4	75°	6	5.40	4.45	1.59	14	25.67	26.59	8.43

for lateral convergence are 58.91%, 67.16%, and 95.80%, and the increments for elliptical aspect ratio are 0.12%, 78.31%, and 103.13%. According to the data mentioned above, under the effect of regional concrete spalling, the vertical convergence value for segment lining increases significantly in the early loading stage. However, the magnitude for the value of growth rate becomes smoother in the stage approaching to instability; the effect due to regional concrete spalling on the lateral convergence of segment lining is minor in the early loading stage, while the growing rate increases rapidly with the increase of loading step by step and reaches the amplitude of vertical convergence when the loading level comes up to the critical point of instability. Besides in the whole loading process, stable growth rate is being observed for elliptical aspect ratio which is defined to combine with deformation characteristics of vertical and lateral convergence. The corresponding growth rate increases with the increase of concrete spalling range, as a matter of fact, the effect of regional spalling of concrete on the overall deformation of segment lining structure is well reflected.

According to Figures 10 and 11, compared with undamaged segment lining structure, after the emergence of regional concrete spalling, the ultimate bearing capacity is prominently reduced for the segment lining structure. When the range of concrete spalling becomes 45°, 60°, and 75°, the critical collapsing load levels reach up to 15, 15, and 14, respectively, in which the levels are 1, 1, and 2 lower compared with undamaged segment lining structure, and the corresponding reduction rates are, respectively, 6%, 6%, and 13%.

4.3. Analysis of Internal Force for Segment Lining. As shown in Figure 12, the distinction is not significant between the magnitude and the change rate of axial force and bending moment for the 4 groups of test segment. The integral segment lining ring is under compression, and the axial force for the whole ring is observed positive, of which most of the distributions for the magnitude are uniform while the distribution for the magnitude of regional concrete spalling is relatively lower; positive bending moment around the vault and the bottom of the arc is observed while negative bending moment is shown nearby the left and right haunch. The distribution law of axial force and bending moment for segment lining structure has not been changed even regional concrete spalling still exists. However, under identical loading level, the magnitude of axial force and bending moment is relatively lower for damaged segment lining structure under the effect of concrete spalling compared with that for undamaged segment, and difference value increases with the increase of concrete spalling range.

As shown in Figures 13 and 14, terrifically strong positive correlation has been observed between the variation of axial force and bending moment for segment lining structure with the increase of loading, and phased characteristic is also discovered. In the initial elastic stage, basically linear relationship is recorded between the loading level and the corresponding axial force and bending moment; in the plasticity developing stage, the axial force and bending moment are increasing with the increase of loading for the whole segment structure, while minor fluctuation appears due to stress redistribution caused by local damage and failure of segment structure; the magnitude of axial force and bending moment drastically increases after the load level exceeds the critical collapsing point accompanied with some release of internal force due to local structure collapsing. Reversed variation is observed for axial force and bending moment on the vault and the bottom of the arc for the segment ring with vault spalling in the range of 75°, which indicates that the expansion of the segmental concrete spalling range will be accelerated for the collapsing process.

Because the regional concrete spalling is located on the vault, and on the one hand, the cross-sectional area is reduced by concrete spalling, and consequently, the transmission of axial force between adjacent segments will be affected; on the other hand, the longitudinal joint tends to be damaged due to concrete spalling, and then the interaction between segment rings will be affected as well, and consequently, additional stress due to the stagger-jointed assembly will be reduced. Therefore, the magnitude for the value of structural axial force on the vault is relatively smaller compared with that on other parts.

For further research on the change of internal force for different groups of the experiment in both elastic stage and plastic stage, the characteristics of internal force in the demarcation point between elasticity and plasticity are summarized in Table 9. The magnitude of maximum negative bending moment for damaged segment rings due to concrete spalling is relatively smaller compared with that for undamaged segment rings, but the distinction between the magnitude is minor, and the maximum distinction between positive moments is within 5%, while that between negative moments is within 10%; the magnitude for the value of maximum axial force for the damaged segment ring due to

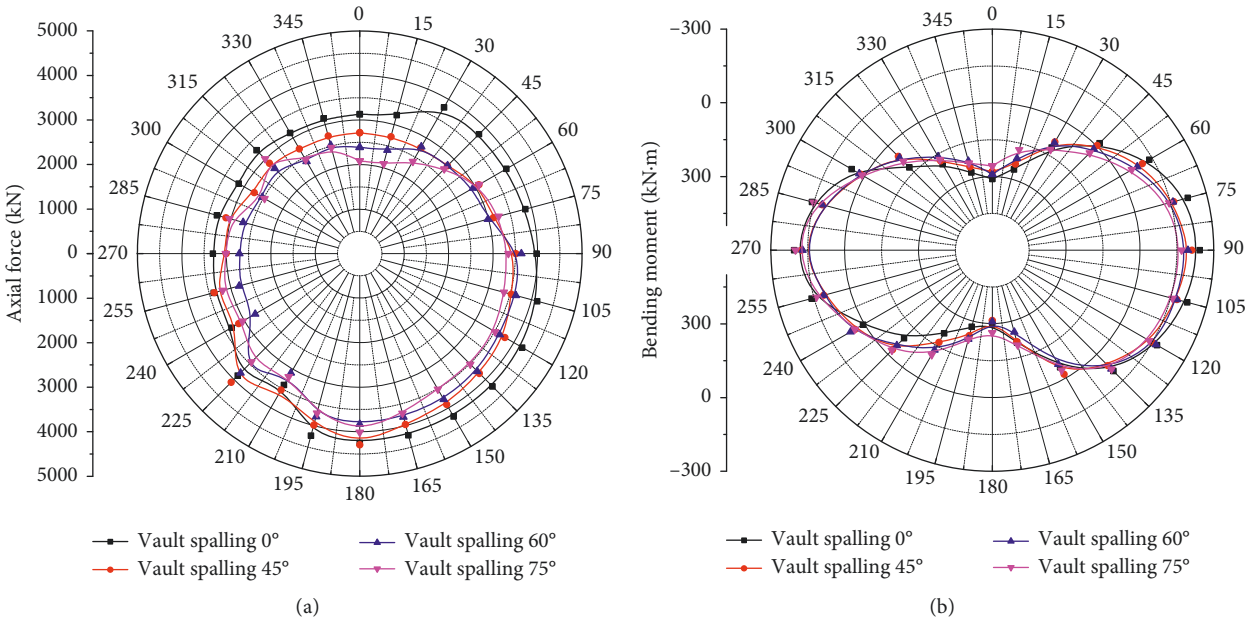

Figure 12: Segment circumferential internal force diagram at elastic-plastic demarcation. (a) Segment circumferential axial force diagram. (b) Segment circumferential bending moment diagram.

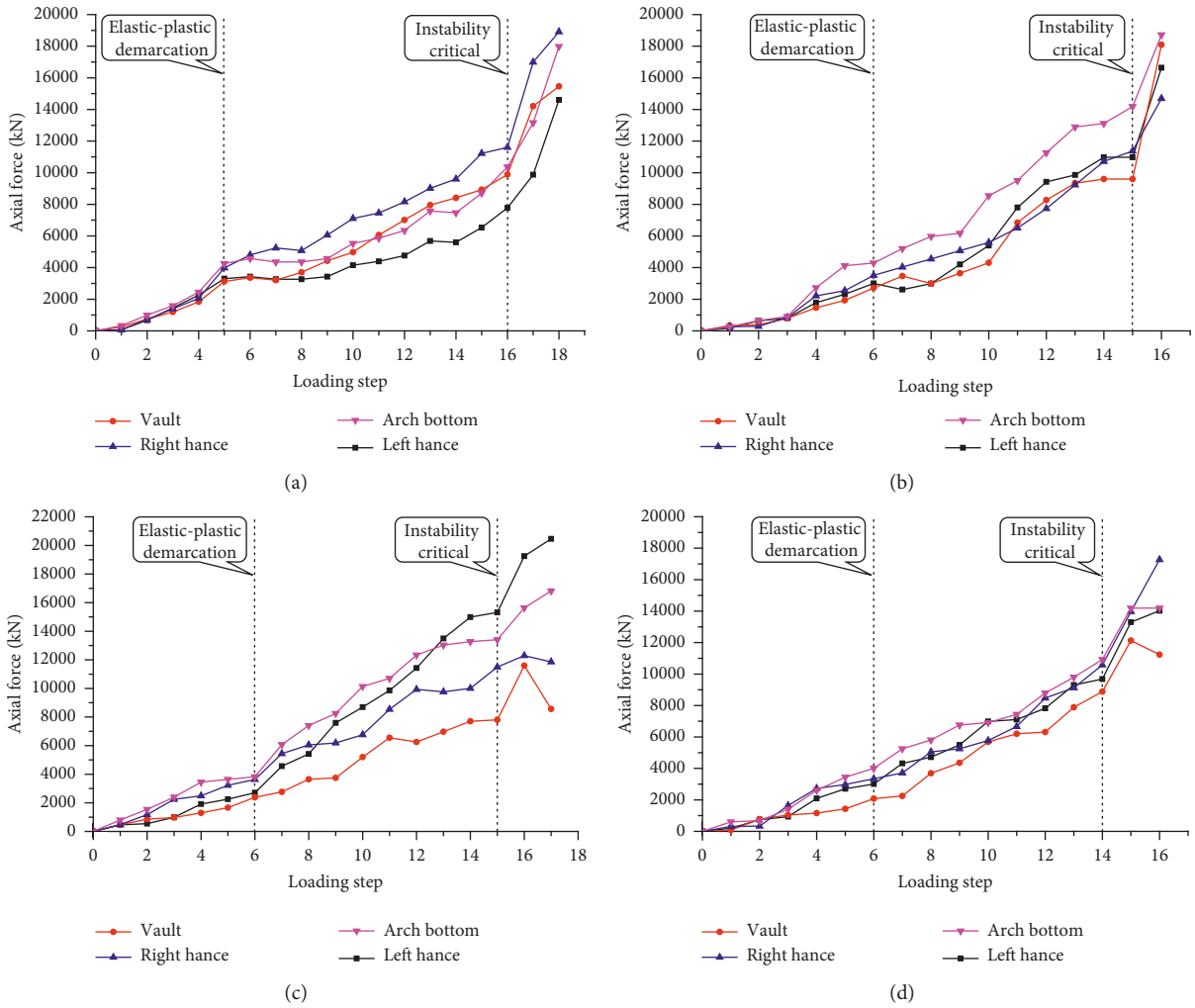

Figure 13: Load-axial force curves at key points of lining. Variation curve of axial force for (a) group 1, (b) group 2, (c) group 3, and (d) group 4.

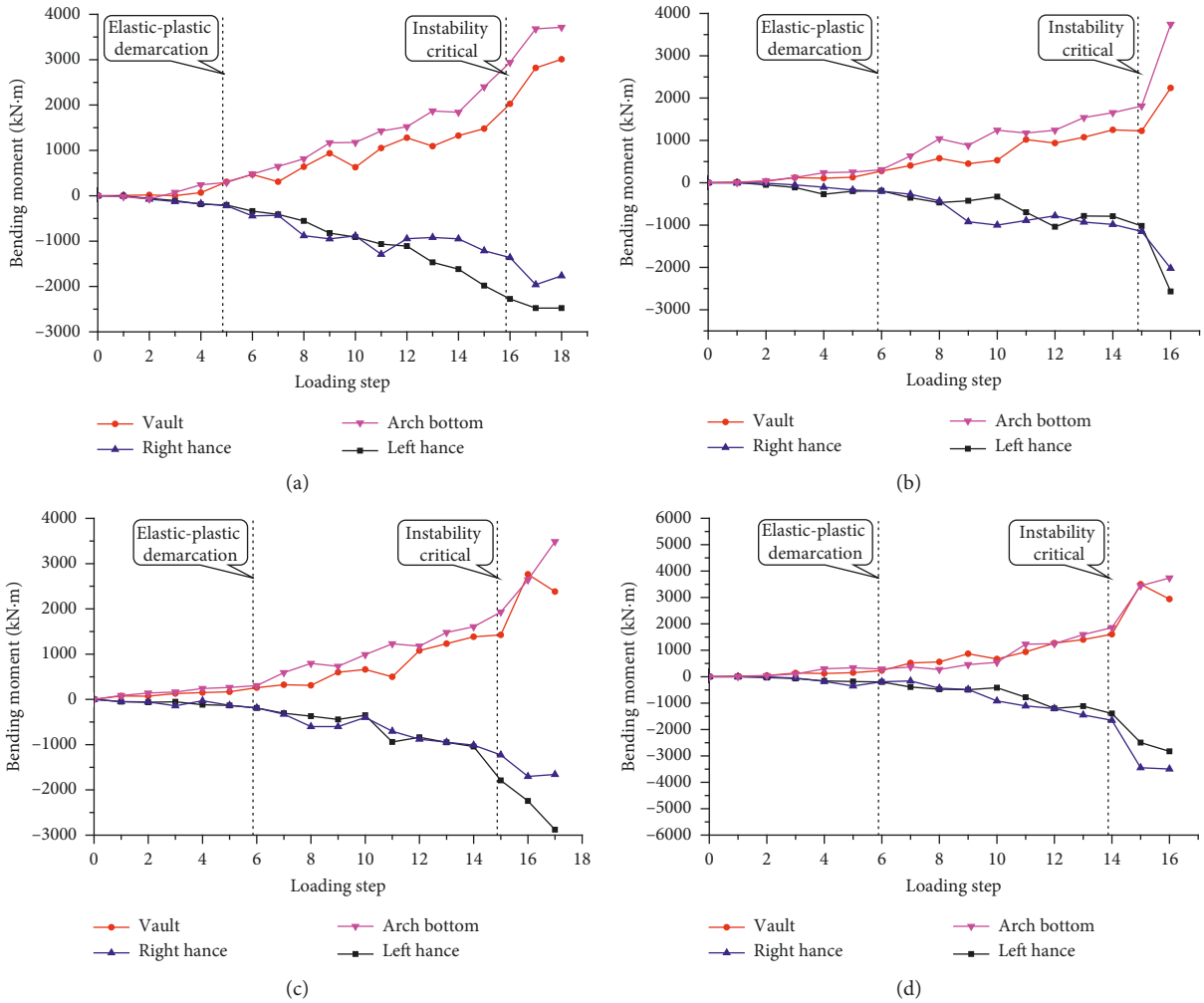

Figure 14: Load-bending moment curves at key points of lining. Variation curve of bending moment for (a) group 1, (b) group 2, (c) group 3, and (d) group 4.

Table 9: Statistics of the internal force features in elastic-plastic demarcation point.

Group number	Range of regional spalling	Loading step at elastic-plastic demarcation point	Internal force in the spalling region		Maximum axial force (kN)	Maximum positive bending moment (kN·m)		Maximum negative bending moment (kN·m)	
			Axial force (kN)	Bending moment (kN·m)		Value	Location	Value	Location
1	None	5	3128	306.5	4250	306.5	Vault	−220.2	Right haunch
2	45°	6	2714	277.4	4292	309.6	Invert	−200.8	Right haunch
3	60°	6	2386	259.1	4033	304.4	Invert	−191.3	Right haunch
4	75°	6	2082	231.6	4012	291.5	Invert	−200.2	Left haunch

concrete spalling is slightly reduced compared with that for undamaged segment rings, and the reduction rate is within 5%. However, all of the value for the axial force of damaged segment rings in the region of concrete spalling is smaller compared with that for undamaged segment rings in the same corresponding place, which leads to the transmission

of maximum positive bending moment from the vault to the bottom of the arc, and with the expansion of concrete spalling range, the value for axial force and bending moment obviously decreases in the region. Compared with undamaged segment rings, the axial force of damaged area decreases by 13.2%, 23.7%, and 33.4% when the concrete spalling ranges reach 45°, 60°, and 75°, and bending moment is reduced by 9.5%, 15.5%, and 24.4%, respectively.

Generally speaking, on the one hand, the effective cross-sectional area for segment structure will be reduced by regional concrete spalling, of which the bending stiffness of the segment is reduced as well, and furthermore, the magnitude of the bending moment for the structure will also be decreased; on the other hand, the transmission of internal force between adjacent segments is affected by regional concrete spalling, and the damage on longitudinal joint will be more likely caused under the action of external load, which affects the interaction between adjacent segment rings, and as a result, the additional stress is reduced as well due to stagger-jointed assembly; finally, the magnitude of axial force will be significantly reduced. It is relatively limited for the influential range of regional concrete spalling on the whole internal force of the structure, most of the distinctions are within 10%, but the variation in axial force and bending moment for the damaged part is prominent due to regional concrete spalling, and the effect on axial force is more obvious than that on bending moment, which could be terrifically undesirable on the structural mechanical behavior; therefore, it has to be necessarily attached importance for this kind of disease.

5. Conclusion

This thesis is based on some metro project, according to the field investigation of regional concrete spalling for the segments, and the mechanical characteristics of segment lining structure in shield tunnel were analyzed and compared by similarity model test under different concrete spalling ranges. The main conclusions can be summarized as follows:

(1) Compared with undamaged segment rings, the integral structure stiffness is reduced by regional concrete spalling, while the flexibility of segment rings is increased. The corresponding range of elastic bearing stage is slightly amplified with the expansion of segmental concrete spalling range while the range of plastic bearing stage is drastically decreased. Sudden changes have been discovered in the process of the damage and failure of segment lining structure.

(2) The numbers of steps are obviously decreased for the accumulated event numbers of acoustic emission with the increase of load step as the range of concrete spalling continues to expand, and the step height is gradually increased, when the ranges of concrete spalling reach 45°, 60°, and 75°. The accumulated event numbers of acoustic emission increase by 34.9%, 45.8%, and 112.3% on the critical collapsing point.

(3) Compared with undamaged segment rings, the magnitude for deformation is significantly increased for damaged segment due to regional concrete spalling under the action of identical external load, when the range of concrete spalling reaches 45°, 60°, and 75°. The vertical convergence value will increase by 143.43%, 198.86%, and 208.57% on the plastic-elastic demarcation point, respectively, the lateral convergence value increases by 3.92%, 7.04%, and 16.2%, and the elliptical aspect ratio increases, respectively, by 47.78%, 66.67%, and 76.67%; meanwhile, the vertical convergence value increases by 83.17%, 91.42%, and 95.30% on the critical collapsing point, the lateral convergence value increases by 58.91%, 67.16%, and 95.80%, and the elliptical aspect ratio increases by 70.12%, 78.31%, and 103.13%.

(4) Compared with undamaged segment lining structure, after the emergence of the disease due to regional concrete spalling, the ultimate bearing capacity is prominently decreased for the segment lining structure, when the range of concrete spalling reaches 45°, 60°, and 75°, and the corresponding reduction rate for ultimate bearing capacity reaches 6%, 6%, and 13%.

(5) The distribution law of axial force and bending moment for segment lining is not changed under the effect of regional concrete spalling, under identical load level, the value magnitude of axial force and bending moment for damaged segment due to concrete spalling is comparatively smaller than that for undamaged segment rings, and the difference value is increased with the increase of concrete spalling range.

(6) The effect of regional concrete spalling is limited on the range of the global internal force, mostly within 10%, while the variation of axial force and bending moment is significantly great due to regional concrete spalling, when the corresponding range of concrete spalling becomes 45°, 60°, and 75°. Respectively, the axial force decreases by 13.2%, 23.7%, and 33.4% in the damaged area of segment rings, while the corresponding bending moment decreases by 9.5%, 15.5%, and 24.4%, and the effect on axial force is much more conspicuous than that on bending moment, which could be extraordinarily unfavorable on the structural mechanical behavior.

Data Availability

The data used to support the findings of this study are available from the corresponding author upon request.

Conflicts of Interest

The authors declare that they have no conflicts of interest.

Acknowledgments

This work was supported by the National Natural Science Foundation of China (grant no. 51578461) and the National Key Research and Development Program of China (grant no. 2016YFC0802202).

References

[1] F. Zhang, H. Zhu, and D. Fu, *Shield Tunnlling Method*, China Communications Press, Beijing, China, 2004.

[2] K. Bian, J. Liu, M. Xiao, and Z. Liu, "Cause investigation and verification of lining cracking of bifurcation tunnel at Huizhou pumped storage power station," *Tunnelling and Underground Space Technology*, vol. 54, pp. 123–134, 2016.

[3] Z. Huang, H. Fu, W. Chen, J. Zhang, and H. Huang, "Damage detection and quantitative analysis of shield tunnel structure," *Automation in Construction*, vol. 94, pp. 303–316, 2018.

[4] X. Li, X. Lin, H. Zhu, X. Wang, and Z. Liu, "Condition assessment of shield tunnel using a new indicator: the tunnel serviceability index," *Tunnelling and Underground Space Technology*, vol. 67, pp. 98–106, 2017.

[5] C. Leung and M. A. Meguid, "An experimental study of the effect of local contact loss on the earth pressure distribution on existing tunnel linings," *Tunnelling and Underground Space Technology*, vol. 26, no. 1, pp. 139–145, 2011.

[6] M. Lei, L. Peng, and C. Shi, "Model test to investigate the failure mechanisms and lining stress characteristics of shallow buried tunnels under unsymmetrical loading," *Tunnelling and Underground Space Technology*, vol. 46, pp. 64–75, 2015.

[7] A. Manuell, G. Niccolini, and C. Alberto, "AE monitoring of a concrete arch road tunnel: damage evolution and localization," *Engineering Fracture Mechanics*, vol. 210, pp. 279–287, 2019.

[8] C. L. Xin, Z. Z. Wang, and B. Gao, "Shaking table tests on seismic response and damage mode of tunnel linings in diverse tunnel-void interaction states," *Tunnelling and Underground Space Technology*, vol. 77, pp. 295–304, 2018.

[9] J. S. Chen and H. H. Mo, "Numerical study on crack problems in segments of shield tunnel using finite element method," *Tunnelling and Underground Space Technology*, vol. 24, no. 1, pp. 91–102, 2009.

[10] H. H. Mo and J. S. Chen, "Study on inner force and dislocation of segments caused by shield machine attitude," *Tunnelling and Underground Space Technology*, vol. 23, no. 3, pp. 281–291, 2008.

[11] C. He, C. Liu, S. Wang et al., "Influence of crack number on mechanical properties of shield tunnel segment structure," *China Journal of Highway and Transport*, vol. 31, no. 10, pp. 210–219, 2018.

[12] C. Liu, C. He, S. Wang et al., "Model test study on failure mode of segment structure of shield tunnel with crack length," *Journal of Central South University (Science and Technology)*, vol. 50, no. 6, pp. 1447–1456, 2019.

[13] K. Feng, C. He, Y. Fang, and Y. Jiang, "Study on the mechanical behavior of lining structure for underwater shield tunnel of high-speed railway," *Advances in Structural Engineering*, vol. 16, no. 8, pp. 1381–1399, 2016.

[14] Y. Fang, H. Wang, J. Guo, Z. Chen, and C. Wu, "Study on the mechanical behavior and the model test of segmental linings for the shield tunnel undercrossing the yellow river," *Procedia Engineering*, vol. 166, pp. 19–31, 2016.

[15] X. Liu, Z. Liu, Y. Ye, Y. Bai, and Y. Zhu, "Mechanical behavior of quasi-rectangular segmental tunnel linings: further insights from full-scale ring tests," *Tunnelling and Underground Space Technology*, vol. 79, pp. 304–318, 2018.

[16] X. Liu, Z. Jiang, Y. Yuan, and H. A. Mang, "Experimental investigation of the ultimate bearing capacity of deformed segmental tunnel linings strengthened by epoxy-bonded steel plates," *Structure and Infrastructure Engineering*, vol. 14, no. 6, pp. 685–700, 2017.

[17] L. Zhou, Z. Zhu, Y. Dong, Y. Fan, Q. Zhou, and S. Deng, "The influence of impacting orientations on the failure modes of cracked tunnel," *International Journal of Impact Engineering*, vol. 125, pp. 134–142, 2019.

[18] S. Wang, Q. Yu, B. Peng et al., "Model study on the effect of cavity on the force and damage of shield tunnel structure," *Journal of Geotechnical Engineering*, vol. 39, no. 1, pp. 89–98, 2017.

[19] S. Wang, G. Yao, X. He et al., "Research on the mechanical property and failure mode of shield tunnels with different hydraulic pressure by model test," *China Civil Engineering Journal*, vol. 51, no. 4, pp. 111–120, 2018.

[20] S. Kohno, A. H.-S. Ang, and W. H. Tang, "Reliability evaluation of idealized tunnel systems," *Structural Safety*, vol. 11, no. 2, pp. 81–93, 1992.

[21] Y. Zhang, M. Zeiml, C. Pichler, and R. Lackner, "Model-based risk assessment of concrete spalling in tunnel linings under fire loading," *Engineering Structures*, vol. 77, pp. 207–215, 2014.

[22] Y. Luo, F. Gong, D. Liu, S. Wang, and X. Si, "Experimental simulation analysis of the process and failure characteristics of spalling in D-shaped tunnels under true-triaxial loading conditions," *Tunnelling and Underground Space Technology*, vol. 90, pp. 42–61, 2019.

[23] F.-Q. Gong, Y. Luo, X.-B. Li, X.-F. Si, and M. Tao, "Experimental simulation investigation on rockburst induced by spalling failure in deep circular tunnels," *Tunnelling and Underground Space Technology*, vol. 81, pp. 413–427, 2018.

[24] G. Xu, S. Wang, G. Dai et al., "Research on ring simulation method of shield tunnel based on internal and external slotting," *Journal of Railway Society*, vol. 38, no. 4, pp. 90–97, 2016.